Redox Biology 59 (2023) 102570

Contents lists available at ScienceDirect

Redox Biology

journal homepage: www.elsevier.com/locate/redox

Decreased autophagosome biogenesis, reduced NRF2, and enhanced ferroptotic cell death are underlying molecular mechanisms of non-alcoholic fatty liver disease

Pengfei Liu [a,b,c,1], Annadurai Anandhan [a,1], Jinjing Chen [a], Aryatara Shakya [a], Matthew Dodson [a], Aikseng Ooi [a], Eli Chapman [a], Eileen White [d], Joe GN. Garcia [e], Donna D. Zhang [a,f,*]

[a] Department of Pharmacology and Toxicology, College of Pharmacy, University of Arizona, Tucson, AZ, 85721, USA
[b] National & Local Joint Engineering Research Center of Biodiagnosis and Biotherapy, The Second Affiliated Hospital of Xi'an Jiaotong University, Xi'an, China
[c] International Joint Research Center on Cell Stress and Disease Diagnosis and Therapy, The Second Affiliated Hospital of Xi'an Jiaotong University, Xi'an, China
[d] Department of Molecular Biology and Biochemistry, Rutgers Cancer Institute of New Jersey, New Brunswick, NJ, USA
[e] Department of Medicine and Arizona Health Sciences Center, University of Arizona, Tucson, AZ, 85721, USA
[f] The University of Arizona Cancer Center, University of Arizona, Tucson, AZ, 85721, USA

ARTICLE INFO

Keywords:
NRF2
KEAP1
High fat diet
Autophagy
Ferroptosis
Liver steatosis
NAFLD
ATG7
mTOR
AKT
AMPK
Fatty acids

ABSTRACT

Background and aims: Caloric excess and sedentary lifestyles have led to an epidemic of obesity, metabolic syndrome, and non-alcoholic fatty liver disease (NAFLD). The objective of this study was to investigate the mechanisms underlying high fat diet (HFD)-induced NAFLD, and to explore NRF2 activation as a strategy to alleviate NAFLD.

Approach and results: Herein, we demonstrated that high fat diet (HFD) induced lipid peroxidation and ferroptosis, both of which could be alleviated by NRF2 upregulation. Mechanistically, HFD suppressed autophagosome biogenesis through AMPK- and AKT-mediated mTOR activation and decreased ATG7, resulting in KEAP1 stabilization and decreased NRF2 levels in mouse liver. Furthermore, ATG7 is required for HFD-induced NRF2 downregulation, as ATG7 deletion in Cre-inducible ATG7 knockout mice decreased NRF2 levels and enhanced ferroptosis, which was not further exacerbated by HFD. This finding was recapitulated in mouse hepatocytes, which showed a similar phenotype upon treatment with saturated fatty acids (SFAs) but not monounsaturated fatty acids (MUFAs). Finally, NRF2 activation blocked fatty acid (FA)-mediated NRF2 downregulation, lipid peroxidation, and ferroptosis. Importantly, the HFD-induced alterations were also observed in human fatty liver tissue samples.

Conclusions: HFD-mediated autophagy inhibition, NRF2 suppression, and ferroptosis promotion are important molecular mechanisms of obesity-driven metabolic diseases. NRF2 activation counteracts HFD-mediated NRF2 suppression and ferroptotic cell death. In addition, SFA vs. MUFA regulation of NRF2 may underlie their harmful vs. beneficial effects. Our study reveals NRF2 as a key player in the development and progression of fatty liver disease and that NRF2 activation could serve as a potential therapeutic strategy.

1. Introduction

Caloric excess and sedentary lifestyles have led to an imbalance of energy uptake and consumption, resulting in a global epidemic of obesity. Obesity is the main driver of metabolic disease and non-alcoholic fatty liver disease (NAFLD). NAFLD, a leading cause of chronic liver disease, affects up to 25% of the world's adult population [1]. Despite this growing prevalence, the mechanisms that drive NAFLD development and subsequent progression remain poorly understood. NAFLD is a spectrum of progressive liver diseases including simple fatty liver (steatosis), nonalcoholic steatohepatitis (NASH), hepatic fibrosis/cirrhosis, and hepatocellular carcinoma (HCC) [2,3]. Hepatic

* Corresponding author. University of Arizona, College of Pharmacy, 1703 E. Mabel St, Tucson, AZ, 85721, USA.
E-mail address: dzhang@pharmacy.arizona.edu (D.D. Zhang).
[1] Authors contributed equally to this work.

https://doi.org/10.1016/j.redox.2022.102570
Received 23 November 2022; Received in revised form 2 December 2022; Accepted 3 December 2022
Available online 5 December 2022

steatosis, the earliest stage of NAFLD, is prevalent in obese individuals, with the potential to advance to more severe liver diseases, type 2 diabetes mellitus, and other metabolic diseases [4]. While hepatic steatosis is reversible, it can progress to NASH, an irreversible stage. Therefore, reversing steatosis or slowing down its progression to NASH represents an important intervention strategy. The progression of NAFLD from steatosis to NASH is influenced by dietary fats that are rich in saturated fatty acids (SFAs) and cholesterol (i.e., the Western diet) [5,6]. On the other hand, the Mediterranean diet consisting of olive oil, fish, nuts, fruits, vegetables, legumes, and cereals that are rich in monounsaturated fatty acids (MUFAs), has been recognized as a healthy diet that reduces the risk of chronic diseases including NAFLD [7].

Mechanisms of NAFLD progression are multifactorial involving genetic variations, as well as increased lipid peroxidation and oxidative stress, defective hepatic autophagy, and imbalances in gut microbiota [8,9]. The protective role of the transcription factor NRF2 in NAFLD has been studied, but a detailed mechanistic understanding of the relationship between NRF2 and NAFLD is lacking [10–13]. NRF2 mediates the cellular antioxidant defense system through upregulation of ARE-bearing target genes [14]. Under basal conditions, the protein levels of NRF2 are kept low due to ubiquitylation and proteasomal degradation, primarily through the action of the KEAP1-Cullin3-Rbx1 E3 ligase complex. Functionally, KEAP1 acts as a substrate adaptor protein that brings NRF2 to the E3 complex [15–17]. As a result, NRF2 generally has a short half-life because of constant ubiquitylation and proteasomal degradation; however, this can be disrupted by NRF2 activators such as sulforaphane (SF). SF works in a KEAP1-cysteine151 dependent manner, resulting in stabilization of NRF2 and activation of NRF2 regulated pathways. In contrast to short-lived NRF2, KEAP1 has a longer half-life that is controlled through autophagy-lysosomal-dependent degradation, which is generally responsible for removal of old or damaged organelles and misfolded proteins [18]. p62, an autophagy cargo-receptor protein, directly interacts with KEAP1 via a DPSTGE motif (similar to the ETGE-interaction motif in NRF2), and can recruit KEAP1 into the autophagosome [19,20]. Next, the autophagosome merges with the lysosome, and KEAP1 and p62 are degraded by lysosomal proteases. Importantly, conditions or compounds that change the protein level or subcellular localization of p62 can disturb the balance between the KEAP1-p62 vs. KEAP1-NRF2 interaction, resulting in NRF2 activation, as exemplified by p62 overexpression or chronic arsenic treatment in cells [19–21].

Autophagy starts with formation of the phagophore, the maturation of which is dependent upon both the ULK complex and the ATG conjugation system, which work in concert to ensure phagophore formation, expansion, and eventual formation of a mature autophagosome [22,23]. HFD was previously shown to inhibit AMPK activation, promote mTOR activation, and inhibit ULK complex formation, thus suppressing autophagy [24,25]. Autophagy, in turn, regulates lipid metabolism and lipid droplet storage, and dysregulation of this axis has been associated with metabolic disorders [23,26]. Another study showed a reduction of autophagy in both *ob/ob* and HFD-induced obesity mouse models [27]. In addition to HFD-mediated autophagy dysregulation, many recent studies have demonstrated an association between HFD, obesity, and ferroptosis, a form of cell death that is induced by excessive lipid peroxidation and free labile iron accumulation. Along these lines, ferroptosis has been shown to play a role during the development and/or progression of chronic liver diseases including NAFLD [28]. HFD was also shown to cause hepatic lipotoxicity by inducing oxidative stress and lipid accumulation, thus triggering ferroptotic cell death [29]. A recent study also indicated that NRF2 activation improves NAFLD by suppressing ferroptosis [30]. With the explosion of ferroptosis-related research, many crucial players that control ferroptotic cell death have been identified. For instance, inhibition of solute carrier family 7 member 11 (SLC7A11), a subunit of the cystine/glutamate antiporter xCT and NRF2-target gene, sensitizes cells to ferroptosis [31]. Glutathione peroxidase 4, an enzyme that catalyzes the reduction of peroxides at the expense of reduced glutathione, has also been shown to be a key regulator of ferroptosis [32,33]. Furthermore, acyl-CoA synthetase long-chain family member 4 (ACSL4) has been identified as a reliable biomarker, with its expression positively correlating with the sensitivity of cells to ferroptosis [34]. *PTGS2*, the gene encoding COX-2, is also significantly upregulated during ferroptosis [32].

In the current study, we investigated the molecular basis of obesity-driven metabolic liver diseases using HFD-induced NAFLD as a model. We demonstrated the importance of the interplay between HFD, autophagy, NRF2, and ferroptosis in NAFLD development and progression. We found that HFD inhibited autophagosome biogenesis, suppressed NRF2, and promoted ferroptosis both *in vitro* and *in vivo*. Our study also uncovered distinct signaling mechanisms between SFAs and MUFAs. Finally, we showed that NRF2 activation is a promising therapeutic strategy to block ferroptotic cell death, reverse steatosis, and possibly slow down NAFLD progression.

2. Materials and methods

2.1. Chemicals, reagents, and antibodies

Fatty Acid Supplement (F7050), palmitic acid (P0050), palmitoleic acid (P9417), oleic acid (O1383), stearic acid (S4751), sulforaphane (S6317), MTT (M2003), rapamycin (R8781), and ferrostatin-1 (SML0583) were purchased from Sigma-Aldrich. The Amplite™ Colorimetric Aspartate Aminotransferase (AST) Assay Kit (13801) and Amplite™ Colorimetric Alanine Aminotransferase (ALT) Assay Kit (13803) were purchased from AAT Bioquest. Antibodies against NRF2 (1:1000, sc-13032), KEAP1 (1:1000, sc-15246), p62 (1:1000, sc-28359), GPX4 (1:1000, sc-166570), GAPDH (1:3000, sc-32233), as well as the mouse (1:3000, sc-2005), goat (1:3000, sc-2350), and rabbit (1:3000, sc-2004) secondary antibodies conjugated to horseradish peroxidase were purchased from Santa Cruz Biotechnology. The antibodies against SLC7A11 (1:3000, 12691S), AMPK (1:3000, 5831S), pAMPK (1:3000, 2535S), AKT (1:3000, 4691S), pAKT (1:3000, 4060S), mTOR (1:3000, 2983S), and pmTOR (1:3000, 5536S) were purchased from Cell Signaling. The antibodies against LC3 (1:3000, L8918) and ATG7 (1:3000, A2856) were purchased from Sigma. The antibody against 4-HNE (1:200, ab46545) was purchased from Abcam.

2.2. Cell culture

AML12 cells (ATCC, CRL-2254) were cultured using DMEM:F12 Medium (Corning, 15-090-CV) supplemented with 10% fetal bovine serum (Gibco, 26140-079), 10 μg/mL insulin (Sigma, 91077C), 5.5 μg/mL transferrin (Sigma, T8158), 5 ng/mL selenium (Sigma, 229865), and 40 ng/mL dexamethasone (Sigma, D4902). Cells were cultured in a humidified incubator at 37 °C with 5% CO_2. The generation of *Nrf2*$^{-/-}$ cells was performed as reported in our previous studies [35,36], using a pair of sgRNA oligos (sgRNA-A: 5′-AGAATTCCTCCCAATTCAGC-3′; sgRNA-B: 5′-TTACTCATCGATCTCCTCGC-3′) that targeted *Nrf2* coding sequences. Successful knockout was confirmed using sequencing and immunoblot analysis.

2.3. Live cell immunofluorescence microscopy

AML12 cells were seeded in 35 mm glass-bottom dishes. The next day, cells were transfected with the ptfLC3 vector containing mRFP-GFP-LC3 (from Dr. Eileen White's lab, Cancer Institute of New Jersey, Rutgers) using Lipofectamine 3000 (Thermo Fisher Scientific, L3000150) for 24 h, then either left untreated, or treated with 2 mL/L Fatty Acid Supplement for 24 h. Finally, cells were imaged using a Zeiss Observer Z1 microscope using the Slidebook 4.2.0.11 software (Intelligent Imaging Innovations).

2.4. Nile Red and BODIPY staining

Lipid droplet formation and lipid peroxidation were analyzed via Nile Red and BODIPY staining, respectively. Briefly, AML12 cells were washed with 1X PBS, then incubated with 0.1 μg/ml Nile Red (Sigma, 72485) or 1 μM BODIPY 581/591 C11 (Thermo Fisher Scientific, D3861) for 30 min in normal culture medium at 37 °C. Cells were then washed twice with 1X PBS and imaged. For the tissue staining, liver tissue from the indicated groups were fixed in 3.7% paraformaldehyde, rinsed several times with 1X PBS, then 20 μm thick sections were cut using a vibratome (Precisionary Instruments LLC). Tissue sections were then incubated with 1 μg/ml Nile Red or 5 μM BODIPY 581/591 C11 for 30 min in 1X PBS at room temperature and washed twice with 1X PBS. Finally, the tissue sections were mounted with Vectashield (Vector Labs) and imaged.

2.5. Real-time quantitative reverse transcription PCR (qRT-PCR)

Total mRNA was extracted using TRIzol (Invitrogen), and 2 μg of total RNA was used to synthesize cDNA. Mouse Gapdh was used for all normalization, and all experiments were performed in triplicate. The primer sequences (5′-3′) are as follows:

mNrf2-F: CTCAGCATGATGGACTTGGA
mNrf2-R: TCTTGCCTCCAAAGGATGTC
mKeap1-F: GATCGGCTGCACTGAACTG
mKeap1-R: GGCAGTGTGACAGGTTGAAG
mSqstm1(p62)-F: AGGATGGGGACTTGGTTGC
mSqstm1(p62)-R: TCACAGATCACATTGGGGTGC
mAtg7-F: TGACCTTCGCGGACCTAAAGA
m Atg7-R: CCCGGATTAGAGGGATGCTC
mSlc7a11-F: TGGGTGGAACTGCTCGTAAT
mSlc7a11-R: AGGATGTAGCGTCCAAATGC
mGpx4-F: GATGGAGCCCATTCCTGAACC
mGpx4-R: CCCTGTACTTATCCAGGCAGA
mPtgs2-F: TGAGCAACTATTCCAAACCAGC
mPtgs2-R: GCACGTAGTCTTCGATCACTATC
mGapdh-F: AGGTCGGTGTGAACGGATTTG
mGapdh-R: TGTAGACCATGTAGTTGAGGTCA.

2.6. Immunoblot analyses

Cells were harvested in 1X sample buffer (50 mM Tris-HCl pH = 8, 2% SDS, 10% glycerol, 100 mM DTT, and 0.1% bromophenol blue). Lysates were immediately boiled for 5 min and sonicated as reported previously (36). All samples were resolved by SDS-PAGE and transferred onto a nitrocellulose membrane. Following transfer, membranes were blocked with 5% milk and incubated with primary antibodies overnight at 4 °C, followed by incubation with secondary antibody for 1 h at room temperature. Finally, protein bands were visualized using SuperSignal West Femto Maximum Sensitivity Substrate (Thermo Fisher Scientific) and the Azure 600 Imaging System (Azure Biosystems). The results in each group were quantified using ImageJ (National Institutes of Health).

2.7. Animal studies

All mice were handled according to the Guide for the Care and Use of Laboratory Animals, and all protocols were approved by the University of Arizona Institutional Animal Care and Use Committee. In addition, all animals received humane care according to the criteria outlined in the "Guide for the Care and Use of Laboratory Animals" prepared by the National Academy of Sciences and published by the National Institutes of Health (NIH publication 86-23 revised 1985). In this study, $Nrf2^{+/+}$ (wild type, WT) and $Nrf2^{-/-}$ mice in the C57BL/6J background were used. Eight-week-old male mice (25–27g) were randomly allocated to the Ctrl group, SF group, High fat diet group, or High fat diet + SF group. To induce hepatic steatosis, mice in the high fat diet groups were fed a diet containing 60% calories from fat, 20% from protein, and 20% from carbohydrates (Research Diets, D12492) for 20 weeks. Mice in the Ctrl and SF groups received a normal chow diet containing 18% calories from fat, 24% from protein and 58% from carbohydrates (Envigo Teklad Laboratory Diet, 2018). In addition to normal vs. high fat chow, SF (12.5 mg/kg) was administered three times per week intraperitoneally in the SF and High fat diet + SF groups. At the end of the study, all mice were sacrificed, and liver tissue was harvested for immunoblot, immunofluorescence, and histological analysis as per our previous studies [27,35]. In addition to the $Nrf2^{+/+}$ and $Nrf2^{-/-}$ mice, $Ubc\text{-}Cre^{ERT2/+}$ mice (The Jackson Laboratory) and $Atg7^{flox/flox}$ mice (from Dr. Eileen White's lab, Cancer Institute of New Jersey, Rutgers) were bred to generate $Ubc\text{-}Cre^{ERT2/+};Atg7^{flox/flox}$ mice. To induce Cre expression, 8–10 week old mice were intraperitoneally (IP) injected with 200 mg/kg tamoxifen (TAM) dissolved in corn oil for five consecutive days. One week later, mice were started on a high fat diet (Research Diets, D12492).

2.8. Human fatty liver tissues

Paraffin-embedded healthy human liver tissue (n = 18) and fatty liver tissue (n = 20) sections were purchased from Biomax. The expression of NRF2, KEAP1, ATG7, mTOR and pmTOR in the different tissues was detected via immunohistochemistry (IHC). Briefly, sodium citrate buffer (0.01 M, pH = 6.0) was used for antigen retrieval, and endogenous peroxidase activity was blocked using 0.3% H_2O_2. Tissue sections were then blocked in 5% BSA for 30 min, and incubated with primary antibodies overnight at 4 °C. Final secondary staining was performed using the EnVision System-HRP kit (Dako) according to the manufacturer's instructions. Primary antibodies against NRF2 (1:100), KEAP1 (1:100), mTOR (1:200), p-mTOR (1:200), and ATG7 (1:3000).

2.9. Statistical analysis

The results are presented as mean ± SD. Statistical analysis was performed using SPSS 17.0. Unpaired Student's t-tests were applied to compare the means of two groups. One-way ANOVA with Bonferroni's correction was used to compare the means of three or more groups. A p value < 0.05 was considered statistically significant.

3. Results

3.1. NRF2 upregulation alleviates hepatic steatosis and lipid peroxidation induced by HFD in vivo

To gain a deeper understanding of the role of NRF2, lipid peroxidation, and ferroptotic cell death in NAFLD, we used a HFD-induced fatty liver disease model (steatosis) in $Nrf2^{+/+}$ and $Nrf2^{-/-}$ mice. As expected, 20 weeks of HFD induced hepatic steatosis, an effect that was markedly reduced in the SF-treated $Nrf2^{+/+}$ group, but not the SF-treated $Nrf2^{-/-}$ group (Fig. 1A). HFD also significantly increased lipid droplet accumulation, which was alleviated by SF in $Nrf2^{+/+}$, but not $Nrf2^{-/-}$ mice (Fig. 1B). HFD resulted in an increase in body and liver weight as well as the ratio of liver/body weight in both $Nrf2^{+/+}$ and $Nrf2^{-/-}$ groups that was suppressed by SF treatment in an NRF2-dependent manner (Fig. 1C). Serum alanine transaminase (ALT) and aspartate transaminase (AST) levels were enhanced by HFD in both genotypes; however, the fold induction of both enzymes was larger in the $Nrf2^{-/-}$ groups, compared to $Nrf2^{+/+}$ groups. In addition, SF suppressed HFD-induced elevation of ALT and AST only in $Nrf2^{+/+}$ mice (Fig. 1D). HFD also resulted in increased markers of oxidative stress, as indicated by lower glutathione levels (GSH) (Fig. 1E) and enhanced MDA formation (Fig. 1F), both of which were alleviated by SF treatment in the $Nrf2^{+/+}$ but not $Nrf2^{-/-}$ group. As expected, HFD led to increased hepatic lipid peroxidation as measured by BODIPY staining that was suppressed by SF in $Nrf2^{+/+}$ but not $Nrf2^{-/-}$ mice (Fig. 1G). Consistently, HFD enhanced lipid peroxidation, as well as the observed

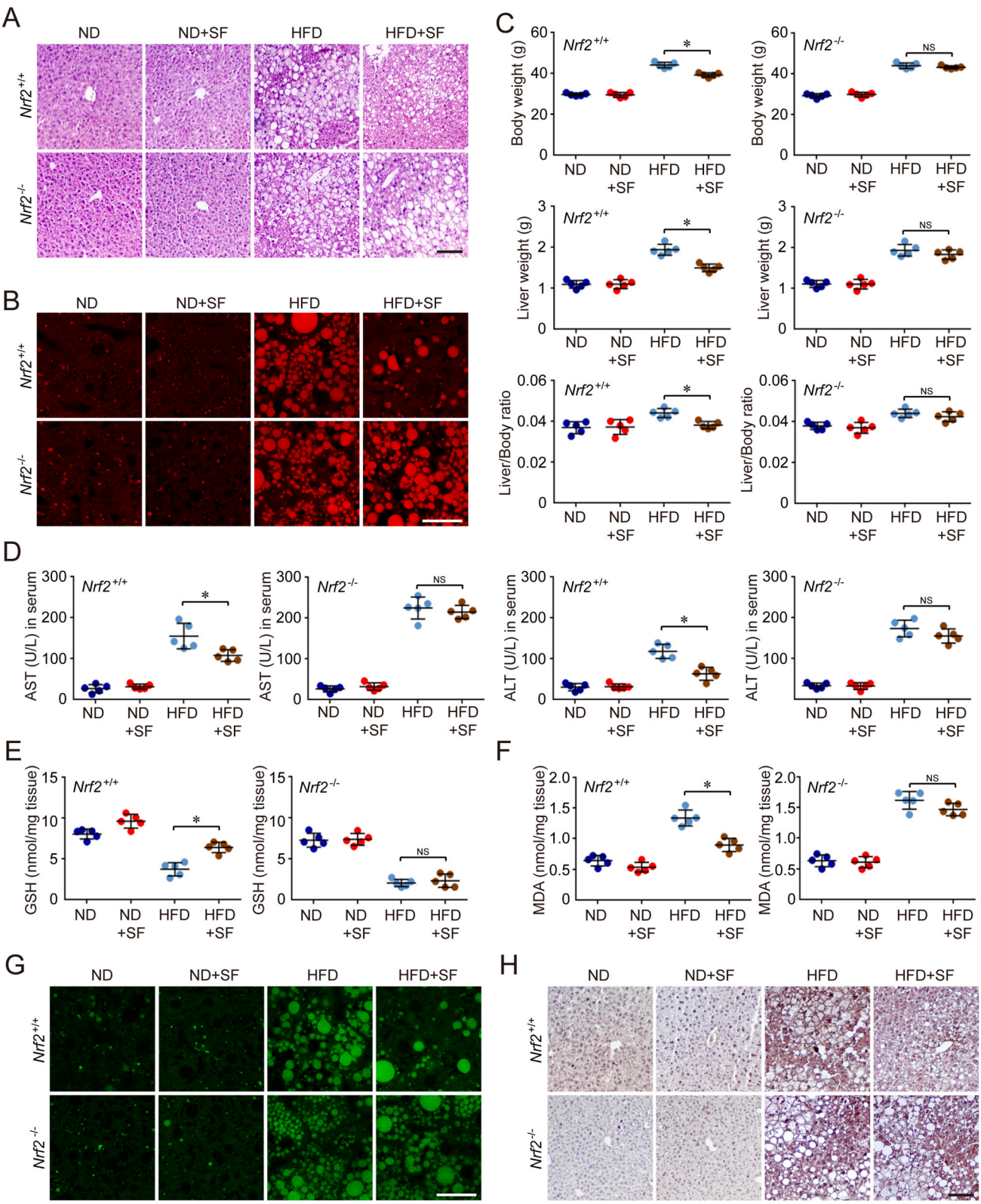

Fig. 1. NRF2 upregulation alleviates hepatic steatosis and lipid peroxidation induced by HFD *in vivo*. *Nrf2*$^{+/+}$ and *Nrf2*$^{-/-}$ mice were fed a normal diet (ND) or high fat diet (HFD) for 20 weeks. Sulforaphane (SF) (12.5 mg/kg) was administered three times per week intraperitoneally in the SF and HFD + SF groups. Liver tissues from each group (n = 5 mice/group) were harvested for analysis. (A) Hematoxylin and eosin staining of the indicated liver tissues. Scale bar = 100 μm. (B) Lipid droplet formation in liver tissues measured using Nile Red staining. Scale bar = 50 μm. (C) Body weight, liver weight, and liver/body weight ratio in each group. (D) Serum AST and ALT levels. (E–F) Oxidative stress was measured by GSH (E) and MDA (F) levels in liver tissues. Results in C–F are expressed as mean ± SD. *$p < 0.05$ compared between two groups. (G) Lipid peroxidation in liver tissues was detected by BODIPY staining. (H) Oxidative damage in liver tissues was measured by IHC analysis of 4-HNE. (For interpretation of the references to colour in this figure legend, the reader is referred to the Web version of this article.)

reduction in the SF-treated *Nrf2*$^{+/+}$ group, were confirmed by 4-HNE staining (Fig. 1H). Collectively, these data indicate that HFD induced lipid peroxidation and liver steatosis and that these phenotypes were alleviated by NRF2 upregulation.

3.2. HFD leads to decreased autophagosome biogenesis, increased KEAP1, decreased NRF2, and enhanced ferroptosis

Interestingly, HFD increased KEAP1 and decreased NRF2 protein levels in the liver of *Nrf2*$^{+/+}$ mice (Fig. 2A). Since KEAP1 is known to be degraded by the autophagy-lysosome pathway through direct KEAP1-p62 interaction, markers of autophagy flux, such as p62, LC3-I/LC3-II, and ATG7 were measured. HFD altered the protein levels of these autophagy-related proteins in an NRF2-independent manner, as the fold of induction for KEAP1 and p62 or reduction for LC3-I/LC3-II and ATG7 were similar regardless of NRF2 status (Fig. 2A for *Nrf2*$^{+/+}$ mice, Fig. 2B for *Nrf2*$^{-/-}$ mice). As expected, SF treatment did not affect any of the proteins controlling the autophagy process (p62, LC3-I/LC3-II, ATG7), nor KEAP1, but significantly induced NRF2 in *Nrf2*$^{+/+}$ mice (Fig. 2A–B). Collectively, these results indicate that autophagosome biogenesis was compromised by chronic HFD, which led to increased KEAP1 and decreased NRF2.

The observation that loss of NRF2-promoted oxidative stress (Fig. 1E and F) and enhanced lipid peroxidation (Fig. 1G and H) in the liver of chronic HFD-fed mice prompted us to test the hypothesis that HFD induced ferroptosis in the livers of these mice. First, induction of lipid peroxidation by HFD in the liver was confirmed by an increased level of 4-HNE-protein adducts that was slightly reduced in the SF-treated group (Fig. 2C–D). Interestingly, ferroptosis biomarkers, including SLC7A11, GPX4, COX2, and ACSL4 were either downregulated (SLC7A11 and GPX4) or upregulated (COX2 and ACSL4) in HFD-fed mice (Fig. 2C–D). Importantly, while HFD induction of ferroptosis is NRF2-independent (Fig. 2C–D), the suppressive effects of SF on HFD-induced alterations to ferroptotic biomarkers are NRF2-dependent (Fig. 2C–D).

3.3. ATG7 depletion is required for HFD-mediated NRF2 downregulation, and NRF2 is critical in determining lipotoxicity, ferroptosis induction, and development of hepatic steatosis

Because HFD resulted in a decrease of both ATG7 and NRF2 in liver tissues, we tested if ATG7 is essential in HFD-mediated NRF2 suppression by using an inducible-Cre ATG7 knockout mouse model. Four weeks of HFD feeding in both *Atg7*$^{+/+}$ (control) and *Atg7*$^{\Delta/\Delta}$ mice (Fig. 3A) recapitulated the changes observed in *Nrf2*$^{+/+}$ mice fed a HFD for 20 weeks, including the development of hepatic steatosis (Fig. 3B), lipid droplet accumulation (Fig. 3C), increased bodyweight and liver/bodyweight ratio (Fig. 3D), elevated serum ALT and AST (Fig. 3E), and enhanced lipid peroxidation (Fig. 3F and G). Interestingly, although the alterations induced by HFD were similar in *Atg7*$^{+/+}$ vs. *Atg7*$^{\Delta/\Delta}$ mice (Fig. 3B–G, compare I vs. II and III vs. IV), reduced expression of ATG7 in *Atg7*$^{\Delta/\Delta}$ mice fed a ND also resulted in hepatic steatosis (Fig. 3B, compare I vs. III, arrow), lipid droplet accumulation (Fig. 3C, compare I vs. III), and increased lipid peroxidation (Fig. 3F and G, compare I vs. III). These results indicated a higher basal level of lipid accumulation and lipid peroxidation. Next, a detailed comparison of the protein level of autophagy, NRF2, and ferroptosis biomarkers (Fig. 3H) revealed the following important points. First, autophagosome biogenesis was compromised in *Atg7*$^{\Delta/\Delta}$ mice, resulting in an increase in KEAP1 and p62, and a reduction of LC3-I/LC3-II (Fig. 3H, compare I vs. III). Second, reduced expression of ATG7 in *Atg7*$^{\Delta/\Delta}$ mice resulted in increased KEAP1 and reduced NRF2 (Fig. 3H, compare I vs. III), Third, ATG7 is required for HFD-mediated KEAP1 accumulation and NRF2 downregulation as the protein levels of NRF2 and KEAP1 remained the same in the ND *Atg7*$^{\Delta/\Delta}$ vs. HFD *Atg7*$^{\Delta/\Delta}$ groups (Fig. 3H compare III vs. IV). Fourth, All the ferroptosis markers (4-HNE, SLC7A11, GPX4, COX2, ACSL4) were altered even in *Atg7*$^{\Delta/\Delta}$ mice fed a ND (Fig. 3I, compare I vs. III). It is worth mentioning, while HFD enhanced 4-HNE in both *Atg7*$^{+/+}$ and *Atg7*$^{\Delta/\Delta}$ mice (Fig. 3G and I), HFD had very limited effect on ferroptosis biomarkers in *Atg7*$^{\Delta/\Delta}$ mice, such as a slight decrease in SLC7A11 and GPX4 levels, but no change in COX-2 and ACSL4 levels (Fig. 3I, compare III vs. IV). These results demonstrate that ATG7 is essential for the downregulation of NRF2 observed in response to HFD and indicates that NRF2 protein levels are a critical determinant of the severity of lipid toxicity, ferroptotic cell death, and degree of liver damage induced by HFD.

3.4. HFD decreases NRF2 and promotes lipid peroxidation in liver tissues in vivo, which is recapitulated in cultured hepatocytes treated with SFAs but not MUFAs

Next, we focused on understanding the molecular basis of HFD-mediated NRF2 inhibition and ferroptosis promotion. A separate experiment in wild type C57/B6 mice fed a ND or HFD reproduced the effects observed in Figs. 2 and 3, including increased KEAP1 and decreased NRF2, SLC7A11, and GPX4 protein levels (Fig. 4A). HFD-mediated NRF2 inhibition and ferroptosis sensitization (decreased SLC7A11 and GPX4) *in vivo* was also validated *in vitro* using a non-transformed mouse hepatocyte cell line (AML12) treated with FA in a dose-dependent manner (Fig. 4B). Interestingly, only the FA supplement, or SFAs such as palmitic acid (16:0, PA) and stearic acid (18:0, SA) (Fig. 4C and D), but not MUFAs such as palmitoleic acid (16:1, PO) and oleic acid (18:1, OA) (Fig. 4E and F), resulted in a dose-dependent increase in KEAP1, and decrease in NRF2, SLC7A11, and GPX4. Consistent with their ability to inhibit NRF2, fatty acids such as PA and SA, but not OA and PO, also decreased GSH (Fig. 4G and H) and increased MDA (Fig. 4I and J). Furthermore, only the FA supplement, or PA and SA alone, resulted in lipid droplet accumulation and lipid peroxidation (Fig. 4K-L).

3.5. HFD alters the AKT- and AMPK-mTOR signaling pathways in liver tissues in vivo, which is recapitulated in cultured hepatocytes treated with SFAs but not MUFAs

Since the nutrient/energy sensor mTOR complex 1 (mTORC1) is crucial in controlling autophagy (phagophore formation) by negatively controlling the ULK complex, the activation status of mTOR and its upstream kinases AMPK and AKT were analyzed in mice fed a HFD and in AML12 cells treated with fatty acids. HFD feeding for 20 weeks significantly enhanced the phosphorylated level of AKT without affecting its total protein levels in liver tissues (Fig. 5A). Contrastingly, AMPK activation was inhibited by HFD, i.e., HFD decreased phosphorylated AMPK without affecting its total protein levels in liver tissues (Fig. 5A). Consistent with previous reports that AKT positively, whereas AMPK negatively, regulates mTORC1, HFD enhanced phosphorylated mTOR without affecting the total level of mTOR in liver tissues (Fig. 5A). These *in vivo* results were recapitulated in *in vitro* in AML12 cells treated with increasing concentrations of a fatty acid supplement (FA) (Fig. 5B). Furthermore, only SFAs (PA and SA) (Fig. 5C and D), but not MUFAs (PO and OA) (Fig. 5E and F) activated AKT, suppressed AMPK, and triggered mTOR activation in a dose-dependent manner.

3.6. HFD downregulates ATG7 and autophagosome biogenesis in liver tissues in vivo, which is recapitulated in cultured hepatocytes treated by SFAs but not MUFAs

The ULK complex and the ATG conjugation system work in concert to ensure phagophore formation, expansion, and eventual formation of a mature autophagosome. Cargo proteins, including KEAP1, are then recruited into the autophagosome by p62, a cargo adapter. In the final step of the autophagy pathway, the autophagosome merges with the lysosome, and KEAP1 and p62 are degraded by lysosomal proteases. The observation that mTOR is activated and ATG7 levels decreased in the

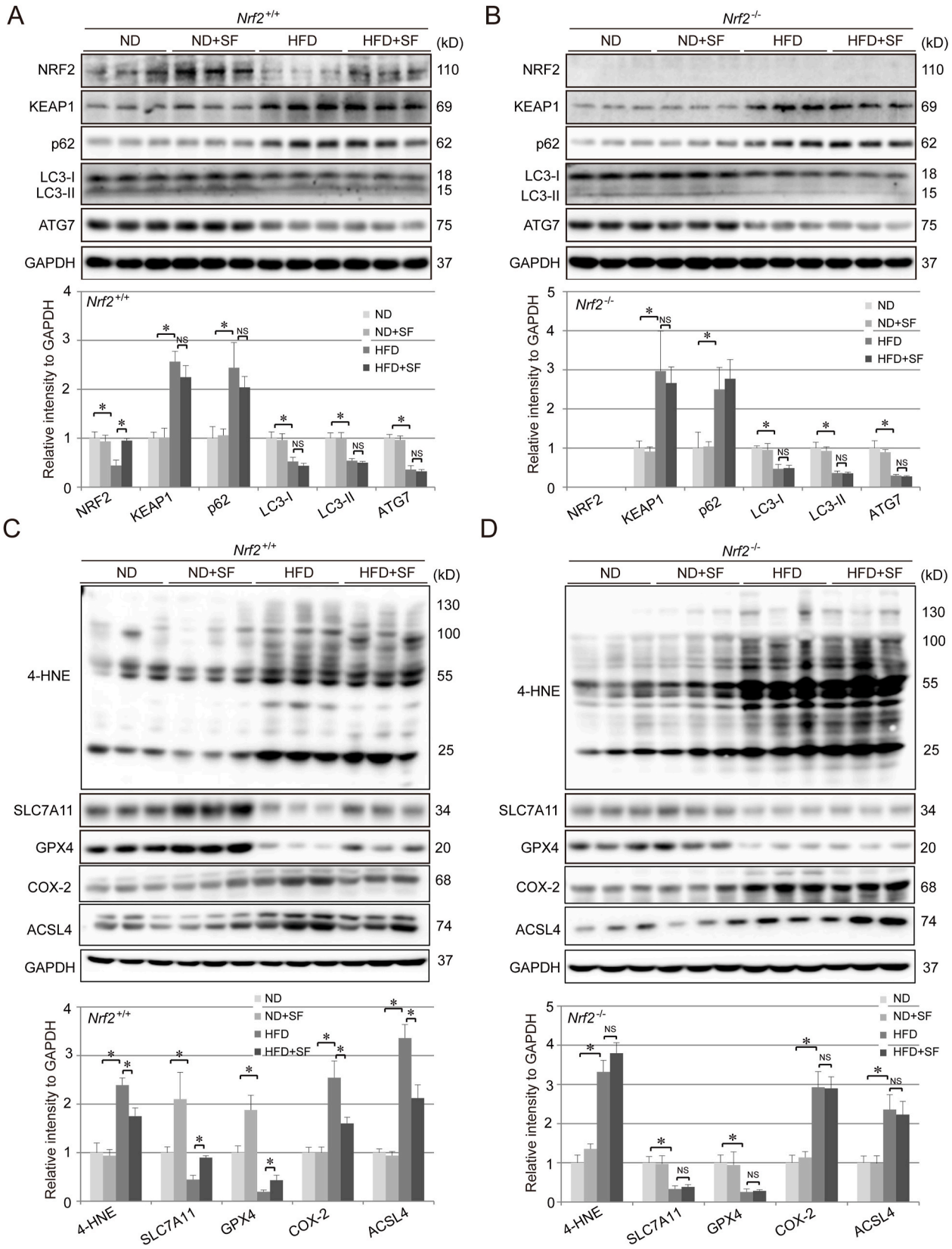

Fig. 2. HFD leads to decreased autophagosome biogenesis, increased KEAP1, decreased NRF2, and enhanced ferroptosis. *Nrf2*$^{+/+}$ and *Nrf2*$^{-/-}$ mice were fed a ND or HFD for 20 weeks with or without SF treatment as described in Fig. 1. (A–D) Protein levels of key players in the NRF2 and autophagy (A–B), or ferroptosis (C–D) cascades in liver tissues were measured using immunoblot analysis. The band intensity for each protein was quantified using ImageJ and relative intensity to GAPDH was plotted as mean ± SD, n = 3 (lower panels). *p < 0.05 compared between two groups.

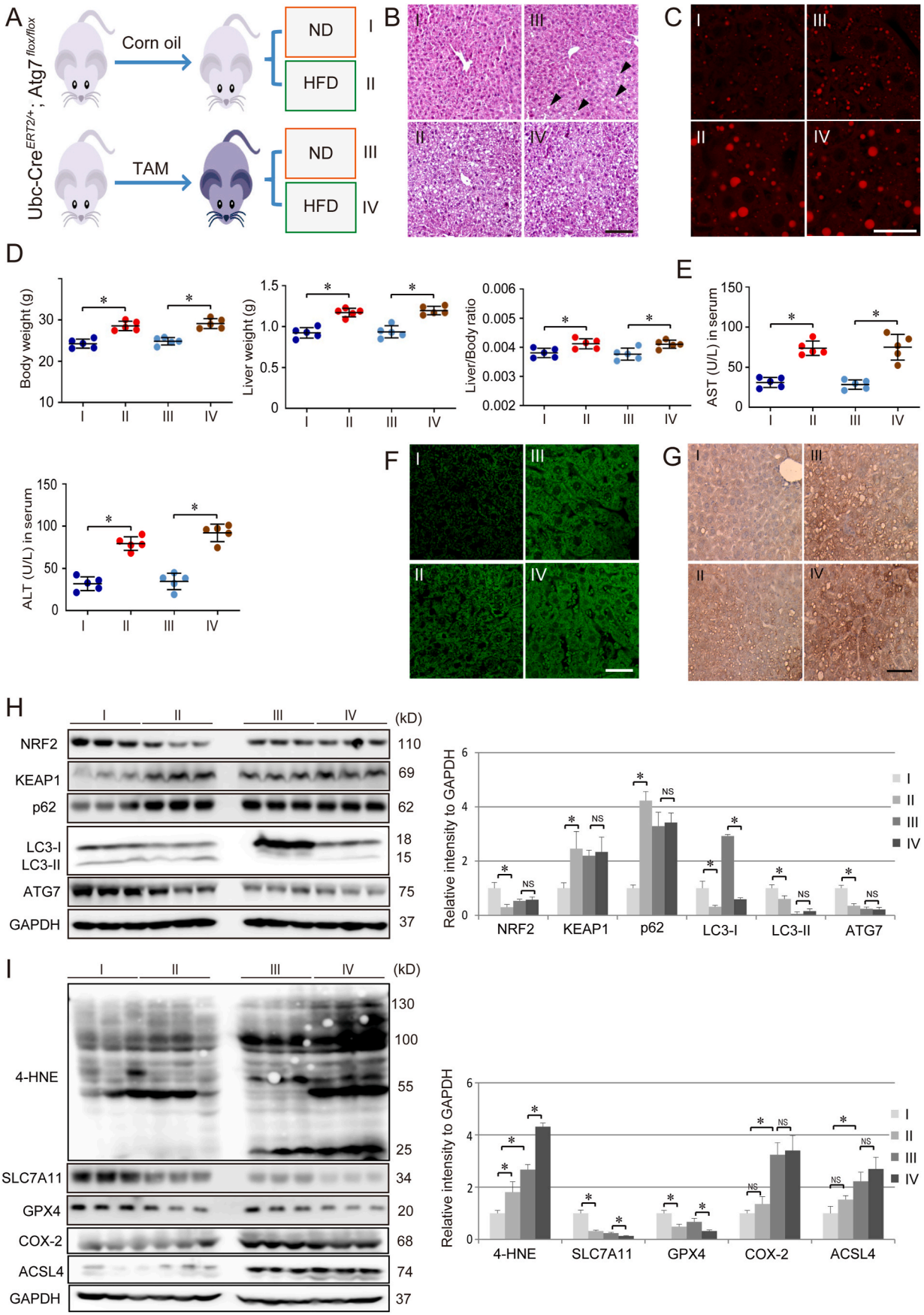

(caption on next page)

Fig. 3. ATG7 is required for HFD-mediated NRF2 downregulation, and NRF2 is critical in determining lipotoxicity, ferroptosis induction, and development of hepatic steatosis. (A) $Atg7^{\Delta/\Delta}$ was induced in *Ubc-Cre*$^{ERT2/+}$;*Atg7*$^{flox/flox}$ mice by tamoxifen (TAM) administration. Six week-old *Ubc-Cre*$^{ERT2/+}$;*Atg7*$^{flox/flox}$ mice received 200 mg/kg TAM ($Atg7^{\Delta/\Delta}$) or corn oil ($Atg7^{+/+}$ control) daily by intraperitoneal injection for five consecutive days. Mice in each group (n = 5) at week eight were fed with ND or HFD for 4 weeks before the liver tissues were harvested. Group I: $Atg7^{+/+}$ mice fed ND; group II: $Atg7^{+/+}$ mice fed HFD; group III: $Atg7^{\Delta/\Delta}$ mice fed ND; and group IV: $Atg7^{\Delta/\Delta}$ mice fed HFD. (B) Hematoxylin and eosin staining of liver tissues. Scale bar = 100 μm. (C) Lipid droplet formation in liver tissues assessed by Nile Red staining. Scale bar = 50 μm. (D) Body weight, liver weight, and liver/body weight ratios in each group. (E) Serum AST and ALT levels in liver tissues from each group. (F–G) Lipid peroxidation in liver tissues was measured by (F) BODIPY and (G) 4-HNE staining. (H–I) Immunoblot analysis of the autophagy pathway (H) and ferroptosis markers (I) in liver tissues. (n = 3 mice/group). Results are expressed as mean ± SD; *$p < 0.05$ compared between two groups. (For interpretation of the references to colour in this figure legend, the reader is referred to the Web version of this article.)

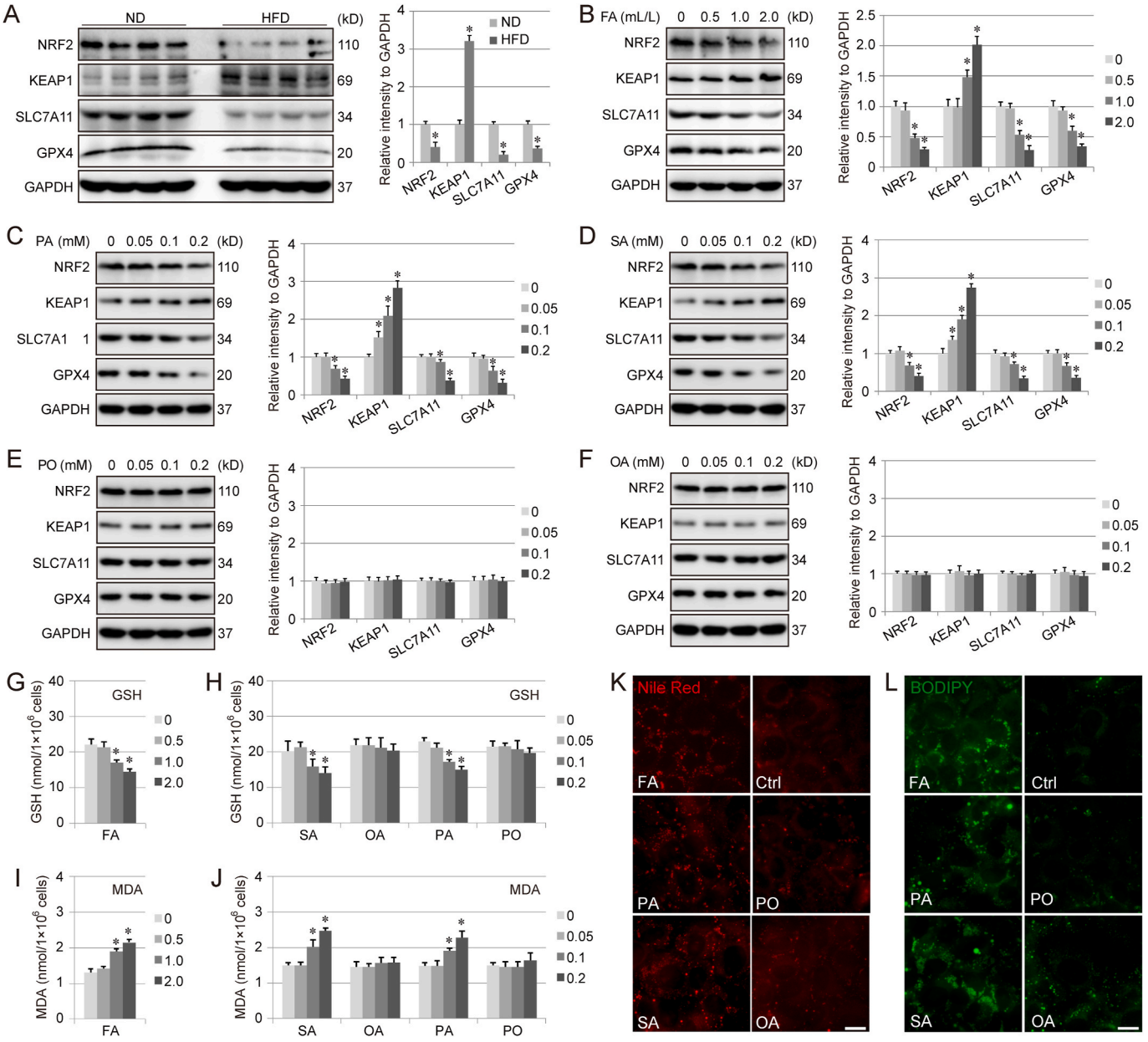

Fig. 4. HFD decreases NRF2 and promotes lipid peroxidation in liver tissues *in vivo*, which is recapitulated in cultured hepatocytes treated with SFAs but not MUFAs. (A) Wild type C57/B6 mice (n = 4 per group) were fed with HFD for 20 weeks, and the liver tissues were harvested for immunoblot analysis. (B–F) AML12 cells were treated with the indicated concentration of mixed fatty acid (FA) supplement, palmitic acid (16:0, PA), stearic acid (18:0, SA), palmitoleic acid (16:1, PO), or oleic acid (18:1, OA) for 24 h. Cell lysates were analyzed using immunoblot analyses. (G–H) The level of GSH in AML12 cells treated with FA (G, the indicated doses in mL/L), or the indicated fatty acid (H, the indicated doses in mM) was measured. (I–J) The same cell lysates were used for MDA measurement. The experiments were repeated 3 times (n = 3). Results are expressed as mean ± SD. *$p < 0.05$ compared with the control (normal diet, 0 ml/L, or 0 mM) group. (K–L) AML12 cells were treated with 2 mL/L FA or 0.2 mM of the indicated fatty acid for 24 h. Lipid droplet formation (K) and lipid peroxidation (L) were detected with Nile Red and BODIPY staining, respectively. (For interpretation of the references to colour in this figure legend, the reader is referred to the Web version of this article.)

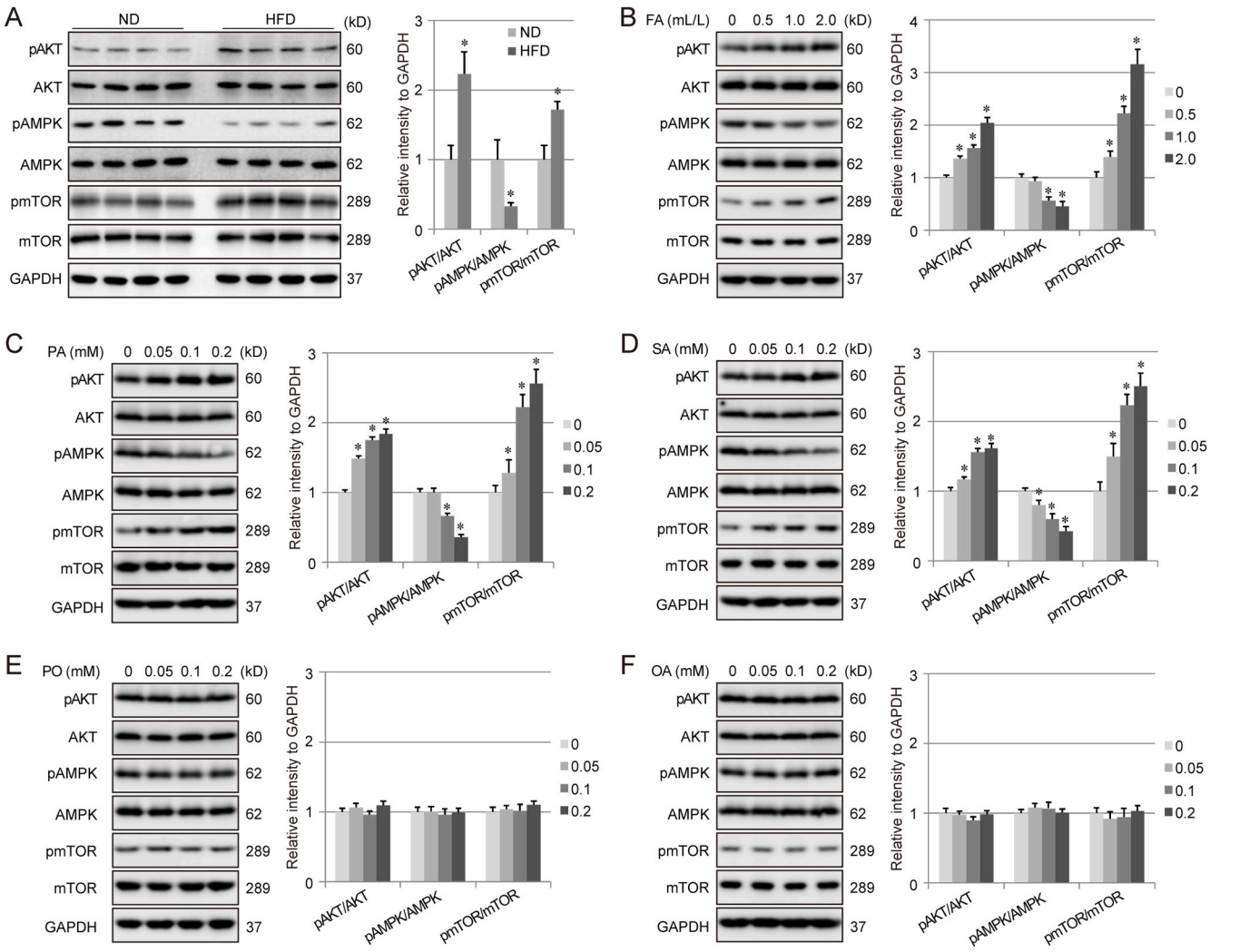

Fig. 5. HFD alters the AKT- and AMPK-mTOR signaling pathways in liver tissues *in vivo*, which is recapitulated in cultured hepatocytes treated with SFAs but not MUFAs. (A) Wild type C57/B6 mice (n = 4 per group) were fed with ND or HFD for 20 weeks, and liver tissues were harvested for immunoblot analysis. (B–F) AML12 cells were treated with the indicated concentrations of FA, palmitic acid (16:0, PA), stearic acid (18:0, SA), palmitoleic acid (16:1, PO), or oleic acid (18:1, OA) for 24 h. Cell lysates were analyzed using immunoblot analysis. The experiments were repeated 3 times (n = 3). Results are expressed as mean ± SD. *p < 0.05 compared with the control (normal diet, 0 ml/L, or 0 mM) group.

liver of mice fed a HFD indicates that autophagosome biogenesis is suppressed. To test this, autophagosome formation was measured in mice fed a HFD as well as AML12 cells treated with fatty acids. Autophagosome formation was decreased in the liver tissue of HFD-mice, as indicated by a reduction of ATG7 and LC3-I/LC3-II, and an increase in the protein levels of p62 (Fig. 6A). This *in vivo* result was recapitulated in *in vitro* using AML12 cells treated with increasing concentrations of FA (Fig. 6B). Furthermore, only SFAs (PA and SA) (Fig. 6C and D), but not MUFAs (PO and OA) (Fig. 6E and F) decreased the protein levels of ATG7 and LC3-I/LC3-II, as well increased p62 protein levels. Next autophagy flux was visualized in AML12 cells transfected with an autophagy tandem fluorescent reporter mRFP-GFP-LC3. In AML12 cells treated with DMSO (Ctrl), PO, and OA, there are numerous yellow and red puncta, indicating a normal basal level of autophagy in these cells; in contrast, FA, PA, and SA treatment significantly reduced the number of puncta (Fig. 6G). These results demonstrate that HFD and SFAs (FA, PA, SA) but not MUFAs (PO, OA) suppress autophagosome biogenesis.

3.7. mTOR activation and ATG7 downregulation are two independent early events, leading to decreased autophagosome biogenesis and NRF2 inhibition in response to HFD or SFA treatment

To better understand the signaling events leading to decreased autophagosome biogenesis, decreased NRF2, and increased lipid peroxidation/ferroptosis, the protein and mRNA levels of key players in each cascade were measured at different time points. AKT activation, AMPK inactivation, and mTOR induction were all early events that occurred before 4 h, at a time point when KEAP1 and NRF2 were not affected (Fig. 7A and B). The observed reduction in ATG7 and LC3-I/LC3-II protein levels started at 4 h, reaching their lowest levels at 8 h (Fig. 7C and D). At 8–16 h, a change in NRF2 and KEAP1 protein levels occurred (Fig. 7E and F), followed by a decrease in the anti-ferroptotic proteins SLC7A11 and GPX4 by 16 h (Fig. 7E and F). Furthermore, while fatty acid-induced changes in NRF2, KEAP1, ATG7, and p62 were all at the protein level (i.e., no observable changes in mRNA expression at any timepoint), the mRNA levels of *Slc7a11*, *Gpx4*, and *Ptgs2* (ferroptosis markers) all changed later, occurring ~16–36 h after initial treatment (Fig. 7G and H). Furthermore, AKT activation, AMPK inhibition, and mTOR activation in response to HFD are independent of ATG7, since the effect of HFD on mTOR activation was the same in $Atg7^{+/+}$ vs.

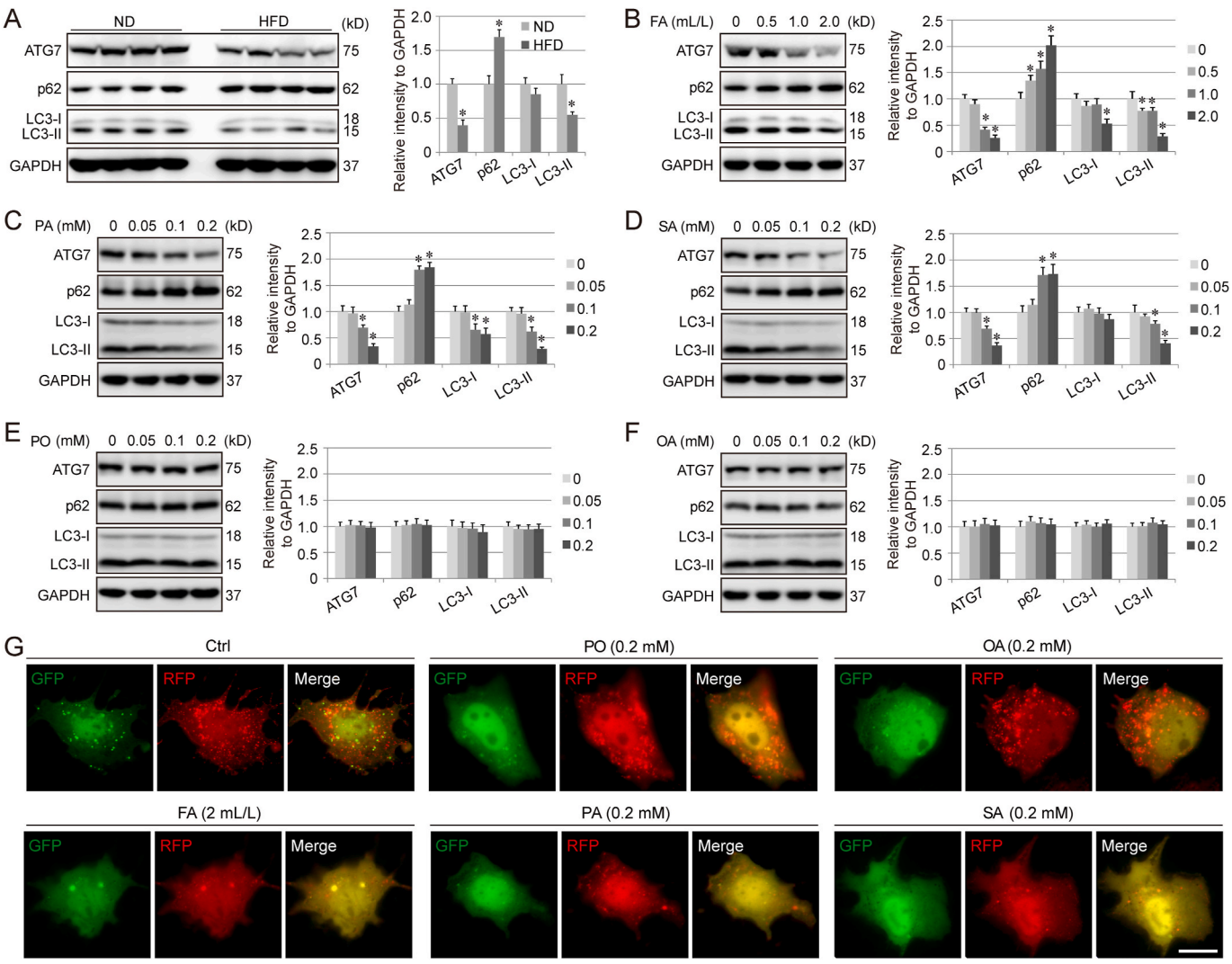

Fig. 6. HFD downregulates ATG7 and autophagosome biogenesis in liver tissues *in vivo*, which is recapitulated in cultured hepatocytes treated by SFAs but not MUFAs. (A) Wild type C57/B6 mice were fed with HFD for 20 weeks, and liver tissues were harvested for immunoblot analysis. (B–F) AML12 cells were treated with the indicated concentration of FA, palmitic acid (16:0, PA), stearic acid (18:0, SA), palmitoleic acid (16:1, PO), or oleic acid (18:1, OA) for 24 h. Cell lysates were analyzed using immunoblot analysis. The experiments were repeated 3 times (n = 3). Results are expressed as mean ± SD. *$p < 0.05$ compared with the control (normal diet, 0 ml/L, or 0 mM) group. (G) AML12 cells were transfected for 24 h with an mRFP-GFP-LC3 plasmid, then treated with the indicated concentrations of various fatty acids for 24 h and imaged. Scale bar = 100 μm.

Atg7$^{\Delta/\Delta}$ mice (Fig. 7I). Collectively, these results support a mode of action whereby HFD or SFA suppress autophagosome biogenesis through both activation of mTOR and downregulation of ATG7, resulting in KEAP1 accumulation and NRF2 degradation that promote HFD-induced lipid peroxidation and ferroptotic cell death (Fig. 7J).

3.8. *mTOR activation, ATG7 downregulation, and NRF2 suppression are also observed in human fatty liver tissues*

To further illustrate the importance of NRF2 in defending against HFD-induced ferroptosis, *Nrf2*$^{-/-}$ AML12 cells were established using Crispr/Cas9. Consistent with the model describing the signaling events of HFD-mediated NRF2 suppression (Fig. 7J), NRF2 deletion had no effect on the kinase activity of AKT, AMPK, or mTOR in response to FA, as expected (Fig. 8A). NRF2 deletion also had no effect on the protein levels of ATG7, LC3-I, or LC3-II in response to FA, although a slight reduction of p62 was observed under both basal and FA-treated conditions (Fig. 8B), which is due to the fact that p62 is an NRF2 target gene [37,38]. Consistent with the notion that HFD suppresses autophagosome biogenesis, FA treatment significantly reduced the number of autophagosomes (puncta), which was observed in both *Nrf2*$^{+/+}$ and *Nrf2*$^{-/-}$ AML12 cells (Fig. 8D). In addition, an increase of KEAP1 in the FA-treated condition was seen even in *Nrf2*$^{-/-}$ AML12 cells (Fig. 8C). These results further verify our model (Fig. 7J), indicating that mTOR activation, ATG7 suppression, and decreased autophagosome biogenesis, are upstream events that mediate NRF2 downregulation in response to FA treatment. In contrast, the level of SLC7A11 or GPX4 in *Nrf2*$^{-/-}$ AML12 cells is much lower than even FA-treated *Nrf2*$^{+/+}$ AML12 cells (Fig. 8C), indicating the importance of NRF2 in regulating the ferroptotic response. Next, we investigated if the *in vivo* protective effect of NRF2 activation by SF on HFD-induced ferroptosis could be replicated in AML12 cells *in vitro*. SF treatment robustly blocked FA-induced NRF2 suppression, as well as the reduction of SLC7A11 and GPX4 (Fig. 8E). As expected, SF treatment had no effect on KEAP1 induction by FA (Fig. 8E). Moreover, while SF treatment did not affect FA-induced lipid droplet accumulation (Fig. 8F), it reduced FA-mediated ferroptosis (Fig. 8F). Ferrostatin-1 (Fer-1), a ferroptosis inhibitor, was included as a control to show that SF blocked FA-induced ferroptosis to a similar degree as Fer-1 (Fig. 8F). Taken together, these data not only further verify the HFD/FA signaling events illustrated in the model (Fig. 7J), but also

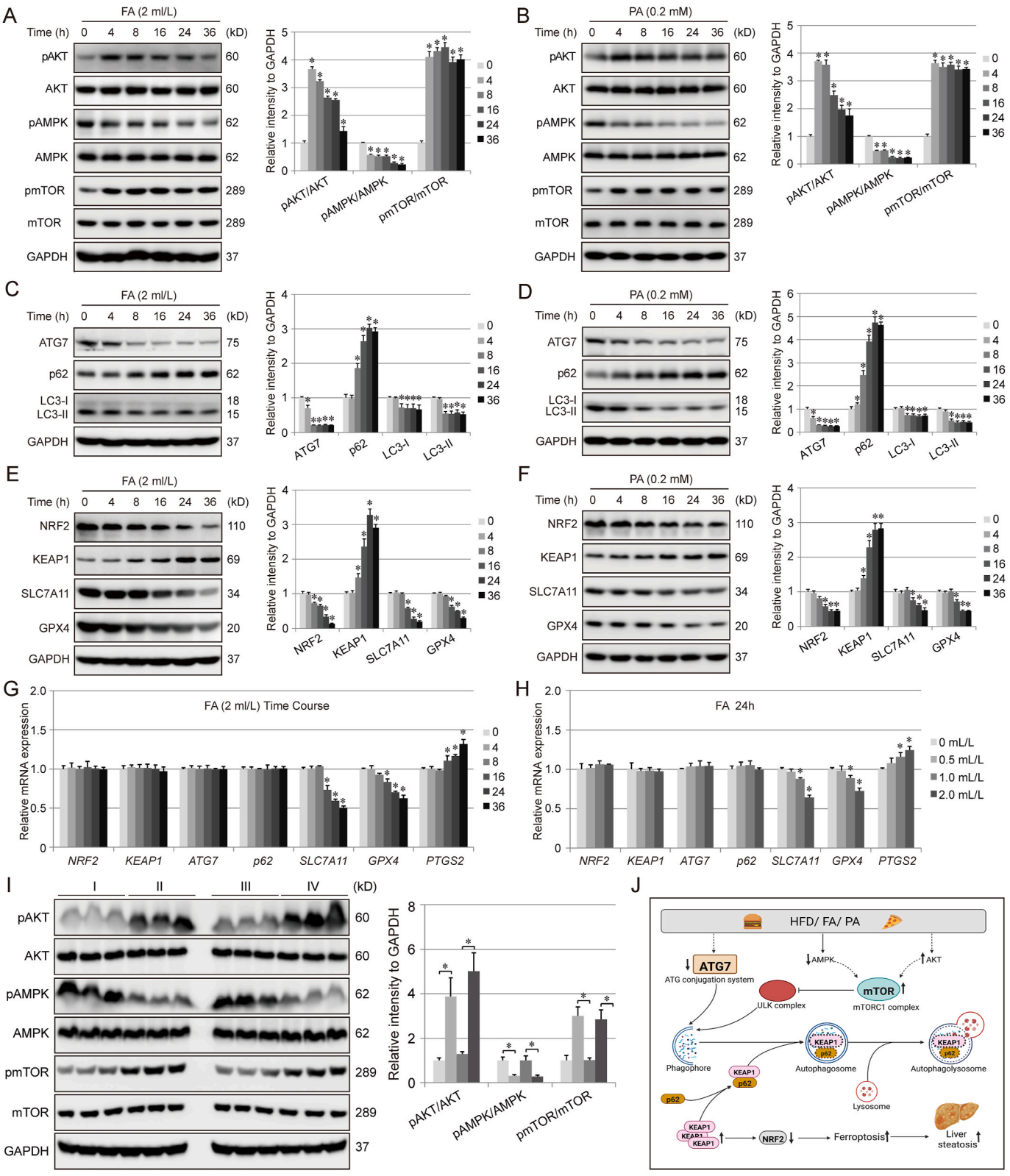

Fig. 7. mTOR activation and ATG7 downregulation are two independent early events, leading to decreased autophagosome biogenesis and NRF2 inhibition in response to HFD or SFA treatment. (A–F) AML12 cells were treated with FA (2 mL/L) or PA (0.2 mM) at the indicated time points. Cells were then harvested for immunoblot analysis. Experiments were repeated three times (n = 3). Results are expressed as mean ± SD. *p < 0.05 different treatment time points compared with untreated control. (G–H) AML12 cells were treated with FA (2 mL/L) for the indicated times (G), or with the indicated dose of FA for 24 h (H), followed by qRT-PCR analysis. (I) The liver tissues from the same experiment described in Fig. 3A were used for immunoblot analysis. (J) Model illustrating how HFD or SFA inhibit autophagosome biogenesis, leading to NRF2 suppression and enhanced ferroptosis during the course of liver steatosis.

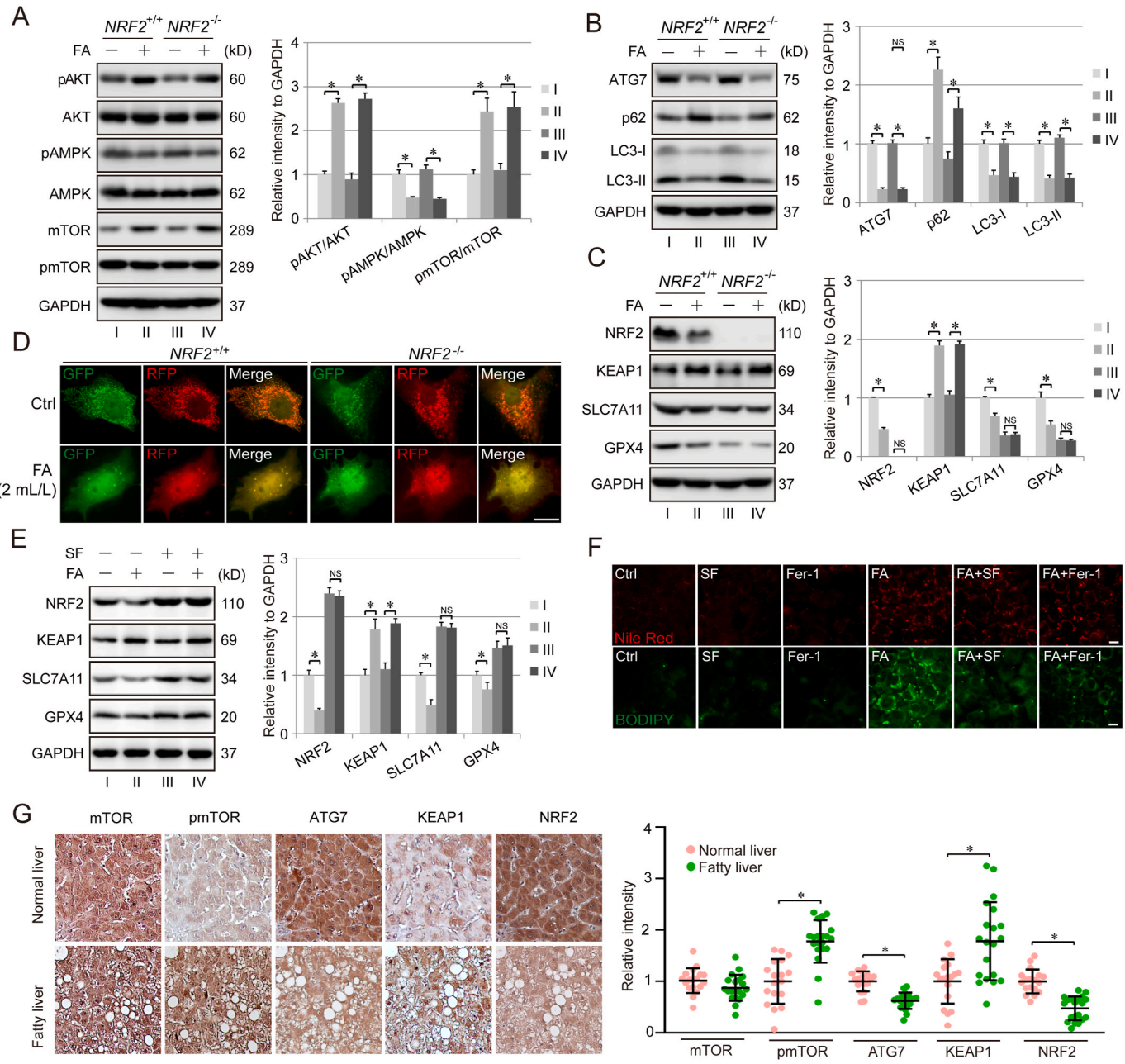

Fig. 8. mTOR activation, ATG7 downregulation, and NRF2 suppression are also observed in human fatty liver tissues. (A–C) *Nrf2*$^{-/-}$ AML12 cells were established using Crispr/Cas9. Both *Nrf2*$^{+/+}$ and *Nrf2*$^{-/-}$ AML12 cells were treated with FA (2 mL/L) for 24 h. The cells were harvested for immunoblot analysis. (D) *Nrf2*$^{+/+}$ and *Nrf2*$^{-/-}$ AML12 cells were transfected with an mRFP-GFP-LC3 plasmid for 24 h, then treated with FA (2 mL/L) for 24 h, followed by live cell imaging. (E) *Nrf2*$^{+/+}$ AML12 cells were cotreated with SF (5 μM) and FA (2 mL/L) for 24 h before the cells were harvested for immunoblot analysis. (F) *Nrf2*$^{+/+}$ AML12 cells were treated for 24 h with SF (2 μM), Fer-1 (5 μM), or FA (2 mL/L) individually or in combination as indicated before cells were fixed and stained with Nile Red or BODIPY. Scale bar = 100 μm. (G) Representative IHC images and the relative intensity analysis of protein expression in human normal liver tissues (n = 18) vs. fatty liver tissues (n = 20). Results are expressed as mean ± SD. *p < 0.05 compared between two groups. (For interpretation of the references to colour in this figure legend, the reader is referred to the Web version of this article.)

confirm that NRF2 upregulation is beneficial to suppress FA-mediated ferroptotic cell death. To verify the human relevance of our findings that HFD/FA suppresses autophagosome biogenesis, resulting in NRF2 suppression and enhanced ferroptosis, paraffin-embedded human liver specimens were analyzed by IHC. While the mTOR intensity was similar between normal vs. fatty liver tissues, the intensity of phosphorylated mTOR was significantly higher in fatty liver tissues compared to normal liver tissues (Fig. 8G). In addition, a decrease of ATG7 and NRF2, as well as an increase of KEAP1 were detected in fatty liver tissues compared to normal liver tissues (Fig. 8G). Therefore, NRF2 downregulation is likely a crucial event during the development of NAFLD in human patients.

4. Discussion

In this study, we investigated the molecular basis of obesity-induced liver diseases using chronic HFD-induced NAFLD as a model. We found that HFD/FA/SFA was able to suppress autophagosome formation through both mTOR activation and ATG7 inhibition. Lipophagy is a selective form of autophagy that is responsible for mediating lipid droplet degradation. Therefore, decreased lipophagy could result in

lipotoxicity such as lipid peroxidation, an essential element of ferroptotic cell death. In addition to enhanced lipid peroxidation, suppression of autophagy stabilizes KEAP1, resulting in a decrease of NRF2 that has anti-ferroptotic functions through the multi-actions of its target genes, including *SLC7A11* and *GCLC/GCLM* that modulate redox balance [39,40], as well as *HERC2/VAMP8* that control ferritin synthesis/degradation, thus maintaining iron homeostasis (manuscript under revision). Therefore, this HFD-mediated double effect on lipid metabolic dysregulation and NRF2 suppression are key drivers of HFD-induced ferroptotic cell death.

Our study has not only revealed the cellular signaling events leading to ferroptotic cell death and liver steatosis in response to HFD/FA/SFA in murine *in vitro* (AML 12 cells) and *in vivo* (HFD-induced mouse liver steatosis) models (Fig. 7J), but also detected these alterations occur in the liver of patients with fatty liver disease (Fig. 8G). Therefore, suppressing these alterations may provide a new clinical avenue for NAFLD intervention. In this study, we have demonstrated NRF2-dependent protection against HFD/FA/SFA-mediated ferroptotic cell death and steatosis using an NRF2-activator, SF (Figs. 1 and 8E and F). As expected, NRF2 activation by SF counteracted HFD-induced molecular alterations, and decreased lipid peroxidation and ferroptosis only in $Nrf2^{+/+}$ but not $Nrf2^{-/-}$ mice, and improved liver function following exposure to a HFD for 20 weeks (Figs. 1–2). NRF2 activation also suppressed FA-induce ferroptotic cell death in an NRF2-dependent manner *in vitro* (Fig. 8E and F). Furthermore, ATG7 depletion was required for HFD-induced NRF2 downregulation, as deletion of ATG7 in Cre-inducible ATG7 knockout mice resulted in decreased NRF2 and a marked increase in ferroptosis, which was only slightly exacerbated by HFD (Fig. 3). This matches previous reports indicating that loss of ATG7 function can dictate the severity of NAFLD in patients [41]. These results also imply that suppression of autophagosome formation is an upstream event leading to NRF2 suppression and enhanced ferroptotic cell death. Another interesting finding is that only mixed FAs or SFAs (PA and SA) but not MUFAs (PO and OA) recapitulated the *in vivo* HFD-mediated signaling events, including mTOR activation, ATG7 reduction, NRF2 suppression, and ferroptosis induction. Although the different health benefits of SFA (bad fat) vs MUFA (good fat) have been well documented, the reason for this difference is not well understood. Currently, the molecular basis of the distinct effects of SFAs vs. MUFAs on NRF2 and ferroptosis is under further investigation.

This study indicates that pharmacological activation of NRF2 may prove to be a promising therapeutic strategy for fatty liver disease intervention. Additionally, our data support the notion that the beneficial effects associated with a diet rich in MUFAs and PUFAs could, at least in part, be via activation of NRF2. This is in agreement with the vast body of scientific literature already generated indicating the protective effects associated with many dietary natural product inducers of this pathway (i.e. sulforaphane – broccoli sprouts, cinnamaldehyde – cinnamon, bixin – achiote, etc …). However, there are no NRF2-specific activators that have been developed into drugs. Dimethyl fumarate (DMF), an FDA approved drug, is a weak and non-specific NRF2 activator [42]. Recently, NRF2-specific activators that are non-electrophilic disruptors of the KEAP1-NRF2 protein-protein interaction, which have less off-target toxicity, are actively under development [43–45]. A compound called KI696, developed by GSK, is a very potent NRF2 inducer, however, the *in vivo* efficacy is limited to ~20 mg/kg in mice [44]. Therefore, developing more potent NRF2 activating drugs with less off-target effects could be valuable for reversing or slowing down the progression of human liver diseases.

Funding information

Research reported was supported by the following grants from the National Institutes of Health: R35ES031575 and P42ES004940 to DDZ, and R01ES031463 to EC, Center grant P30 ES006694.

Author contributions

D.D.Z. and P.L. conceived the project. P.L., A.A., J.C., A.S., and M.D. conducted the experiments and analyzed the data. E.C., A.O., J.G.N.G., and E.W. provided reagents, discussed the project, and edited the manuscript.

Declaration of competing interest

The authors declare no conflicts of interest.

Data availability

Data will be made available on request.

Abbreviations

HFD	high fat diet
NAFLD	non-alcoholic fatty liver disease
NRF2	nuclear factor erythroid 2-related factor 2
KEAP1	Kelch-like ECH-associated protein 1
LC3	microtubule associated protein 1 light chain 3
SFA	saturated fatty acid
MUFA	monounsaturated fatty acid
ALT	alanine aminotransferase
AST	aspartate aminotransferase

References

[1] Z. Younossi, Q.M. Anstee, M. Marietti, T. Hardy, L. Henry, M. Eslam, J. George, E. Bugianesi, Global burden of NAFLD and NASH: trends, predictions, risk factors and prevention, Nat. Rev. Gastroenterol. Hepatol. 15 (1) (2018) 11–20.
[2] L.A. Adams, J.F. Lymp, J. St Sauver, S.O. Sanderson, K.D. Lindor, A. Feldstein, P. Angulo, The natural history of nonalcoholic fatty liver disease: a population-based cohort study, Gastroenterology 129 (1) (2005) 113–121.
[3] Q.M. Anstee, H.L. Reeves, E. Kotsiliti, O. Govaere, M. Heikenwalder, From NASH to HCC: current concepts and future challenges, Nat. Rev. Gastroenterol. Hepatol. 16 (7) (2019) 411–428.
[4] E. Fabbrini, S. Sullivan, S. Klein, Obesity and nonalcoholic fatty liver disease: biochemical, metabolic, and clinical implications, Hepatology 51 (2) (2010) 679–689.
[5] G.E. Arteel, Beyond reasonable doubt: who is the culprit in lipotoxicity in NAFLD/NASH? Hepatology 55 (6) (2012) 2030–2032.
[6] C.Y. Lian, Z.Z. Zhai, Z.F. Li, L. Wang, High fat diet-triggered non-alcoholic fatty liver disease: a review of proposed mechanisms, Chem. Biol. Interact. 330 (2020), 109199.
[7] M.R. Entezari, N. Talenezhad, F. Mirzavandi, S. Rahimpour, H. Mozaffari-Khosravi, H. Fallahzadeh, M. Hosseinzadeh, Mediterranean dietary pattern and non-alcoholic fatty liver diseases: a case-control study, J. Nutr. Sci. 10 (2021) e55.
[8] A.M. Diehl, C. Day, Cause, pathogenesis, and treatment of nonalcoholic steatohepatitis, N. Engl. J. Med. 377 (21) (2017) 2063–2072.
[9] S.L. Friedman, B.A. Neuschwander-Tetri, M. Rinella, A.J. Sanyal, Mechanisms of NAFLD development and therapeutic strategies, Nat. Med. 24 (7) (2018) 908–922.
[10] S. Chowdhry, M.H. Nazmy, P.J. Meakin, A.T. Dinkova-Kostova, S.V. Walsh, T. Tsujita, J.F. Dillon, M.L. Ashford, J.D. Hayes, Loss of Nrf2 markedly exacerbates nonalcoholic steatohepatitis, Free Radic. Biol. Med. 48 (2) (2010) 357–371.
[11] R. Shimozono, Y. Asaoka, Y. Yoshizawa, T. Aoki, H. Noda, M. Yamada, M. Kaino, H. Mochizuki, Nrf2 activators attenuate the progression of nonalcoholic steatohepatitis-related fibrosis in a dietary rat model, Mol. Pharmacol. 84 (1) (2013) 62–70.
[12] P.J. Meakin, S. Chowdhry, R.S. Sharma, F.B. Ashford, S.V. Walsh, R.J. McCrimmon, A.T. Dinkova-Kostova, J.F. Dillon, J.D. Hayes, M.L. Ashford, Susceptibility of Nrf2-null mice to steatohepatitis and cirrhosis upon consumption of a high-fat diet is associated with oxidative stress, perturbation of the unfolded protein response, and disturbance in the expression of metabolic enzymes but not with insulin resistance, Mol. Cell Biol. 34 (17) (2014) 3305–3320.
[13] L.Y. Lee, U.A. Kohler, L. Zhang, D. Roenneburg, S. Werner, J.A. Johnson, D. P. Foley, Activation of the Nrf2-ARE pathway in hepatocytes protects against steatosis in nutritionally induced non-alcoholic steatohepatitis in mice, Toxicol. Sci. 142 (2) (2014) 361–374.
[14] D.D. Zhang, Mechanistic studies of the Nrf2-Keap1 signaling pathway, Drug Metab. Rev. 38 (4) (2006) 769–789.
[15] D.D. Zhang, M. Hannink, Distinct cysteine residues in Keap1 are required for Keap1-dependent ubiquitination of Nrf2 and for stabilization of Nrf2 by chemopreventive agents and oxidative stress, Mol. Cell Biol. 23 (22) (2003) 8137–8151.

[16] D.D. Zhang, S.C. Lo, J.V. Cross, D.J. Templeton, M. Hannink, Keap1 is a redox-regulated substrate adaptor protein for a Cul3-dependent ubiquitin ligase complex, Mol. Cell Biol. 24 (24) (2004) 10941–10953.
[17] A. Kobayashi, M.I. Kang, H. Okawa, M. Ohtsuji, Y. Zenke, T. Chiba, K. Igarashi, M. Yamamoto, Oxidative stress sensor Keap1 functions as an adaptor for Cul3-based E3 ligase to regulate proteasomal degradation of Nrf2, Mol. Cell Biol. 24 (16) (2004) 7130–7139.
[18] K. Taguchi, N. Fujikawa, M. Komatsu, T. Ishii, M. Unno, T. Akaike, H. Motohashi, M. Yamamoto, Keap1 degradation by autophagy for the maintenance of redox homeostasis, Proc. Natl. Acad. Sci. U. S. A. 109 (34) (2012) 13561–13566.
[19] A. Lau, X.J. Wang, F. Zhao, N.F. Villeneuve, T. Wu, T. Jiang, Z. Sun, E. White, D. D. Zhang, A noncanonical mechanism of Nrf2 activation by autophagy deficiency: direct interaction between Keap1 and p62, Mol. Cell Biol. 30 (13) (2010) 3275–3285.
[20] M. Komatsu, H. Kurokawa, S. Waguri, K. Taguchi, A. Kobayashi, Y. Ichimura, Y. S. Sou, I. Ueno, A. Sakamoto, K.I. Tong, M. Kim, Y. Nishito, S. Iemura, T. Natsume, T. Ueno, E. Kominami, H. Motohashi, K. Tanaka, M. Yamamoto, The selective autophagy substrate p62 activates the stress responsive transcription factor Nrf2 through inactivation of Keap1, Nat. Cell Biol. 12 (3) (2010) 213–223.
[21] A. Lau, Y. Zheng, S. Tao, H. Wang, S.A. Whitman, E. White, D.D. Zhang, Arsenic inhibits autophagic flux, activating the Nrf2-Keap1 pathway in a p62-dependent manner, Mol. Cell Biol. 33 (12) (2013) 2436–2446.
[22] Z. Yang, D.J. Klionsky, Mammalian autophagy: core molecular machinery and signaling regulation, Curr. Opin. Cell Biol. 22 (2) (2010) 124–131.
[23] Y. Zhang, J.R. Sowers, J. Ren, Targeting autophagy in obesity: from pathophysiology to management, Nat. Rev. Endocrinol. 14 (6) (2018) 356–376.
[24] Y. Li, Y. Cheng, Y. Zhou, H. Du, C. Zhang, Z. Zhao, Y. Chen, Z. Zhou, J. Mei, W. Wu, M. Chen, High fat diet-induced obesity leads to depressive and anxiety-like behaviors in mice via AMPK/mTOR-mediated autophagy, Exp. Neurol. 348 (2022), 113949.
[25] D.H. Lee, J.S. Park, Y.S. Lee, J. Han, D.K. Lee, S.W. Kwon, D.H. Han, Y.H. Lee, S. H. Bae, SQSTM1/p62 activates NFE2L2/NRF2 via ULK1-mediated autophagic KEAP1 degradation and protects mouse liver from lipotoxicity, Autophagy 16 (11) (2020) 1949–1973.
[26] R. Singh, S. Kaushik, Y. Wang, Y. Xiang, I. Novak, M. Komatsu, K. Tanaka, A. M. Cuervo, M.J. Czaja, Autophagy regulates lipid metabolism, Nature 458 (7242) (2009) 1131–1135.
[27] L. Yang, P. Li, S. Fu, E.S. Calay, G.S. Hotamisligil, Defective hepatic autophagy in obesity promotes ER stress and causes insulin resistance, Cell Metabol. 11 (6) (2010) 467–478.
[28] J. Wu, Y. Wang, R. Jiang, R. Xue, X. Yin, M. Wu, Q. Meng, Ferroptosis in liver disease: new insights into disease mechanisms, Cell Death Dis. 7 (1) (2021) 276.
[29] J.J. Jiang, G.F. Zhang, J.Y. Zheng, J.H. Sun, S.B. Ding, Targeting mitochondrial ROS-mediated ferroptosis by quercetin alleviates high-fat diet-induced hepatic lipotoxicity, Front. Pharmacol. 13 (2022), 876550.
[30] G. Gao, Z. Xie, E.W. Li, Y. Yuan, Y. Fu, P. Wang, X. Zhang, Y. Qiao, J. Xu, C. Holscher, H. Wang, Z. Zhang, Dehydroabietic acid improves nonalcoholic fatty liver disease through activating the Keap1/Nrf2-ARE signaling pathway to reduce ferroptosis, J. Nat. Med. 75 (3) (2021) 540–552.
[31] S.J. Dixon, D.N. Patel, M. Welsch, R. Skouta, E.D. Lee, M. Hayano, A.G. Thomas, C. E. Gleason, N.P. Tatonetti, B.S. Slusher, B.R. Stockwell, Pharmacological inhibition of cystine-glutamate exchange induces endoplasmic reticulum stress and ferroptosis, Elife 3 (2014), e02523.
[32] W.S. Yang, R. SriRamaratnam, M.E. Welsch, K. Shimada, R. Skouta, V. S. Viswanathan, J.H. Cheah, P.A. Clemons, A.F. Shamji, C.B. Clish, L.M. Brown, A. W. Girotti, V.W. Cornish, S.L. Schreiber, B.R. Stockwell, Regulation of ferroptotic cancer cell death by GPX4, Cell 156 (1–2) (2014) 317–331.
[33] J.P. Friedmann Angeli, M. Schneider, B. Proneth, Y.Y. Tyurina, V.A. Tyurin, V. J. Hammond, N. Herbach, M. Aichler, A. Walch, E. Eggenhofer, D. Basavarajappa, O. Radmark, S. Kobayashi, T. Seibt, H. Beck, F. Neff, I. Esposito, R. Wanke, H. Forster, O. Yefremova, M. Heinrichmeyer, G.W. Bornkamm, E.K. Geissler, S. B. Thomas, B.R. Stockwell, V.B. O'Donnell, V.E. Kagan, J.A. Schick, M. Conrad, Inactivation of the ferroptosis regulator Gpx4 triggers acute renal failure in mice, Nat. Cell Biol. 16 (12) (2014) 1180–1191.
[34] H. Yuan, X. Li, X. Zhang, R. Kang, D. Tang, Identification of ACSL4 as a biomarker and contributor of ferroptosis, Biochem. Biophys. Res. Commun. 478 (3) (2016) 1338–1343.
[35] P. Liu, M.R. de la Vega, M. Dodson, F. Yue, B. Shi, D. Fang, E. Chapman, L. Liu, D. D. Zhang, Spermidine confers liver protection by enhancing NRF2 signaling through a MAP1S-mediated non-canonical mechanism, Hepatology 70 (1) (2019) 372–388.
[36] H. Liu, A.A. Kiseleva, E.A. Golemis, Ciliary signalling in cancer, Nat. Rev. Cancer 18 (8) (2018) 511–524.
[37] A. Jain, T. Lamark, E. Sjottem, K.B. Larsen, J.A. Awuh, A. Overvatn, M. McMahon, J.D. Hayes, T. Johansen, p62/SQSTM1 is a target gene for transcription factor NRF2 and creates a positive feedback loop by inducing antioxidant response element-driven gene transcription, J. Biol. Chem. 285 (29) (2010) 22576–22591.
[38] M. Pajares, N. Jimenez-Moreno, A.J. Garcia-Yague, M. Escoll, M.L. de Ceballos, F. Van Leuven, A. Rabano, M. Yamamoto, A.I. Rojo, A. Cuadrado, Transcription factor NFE2L2/NRF2 is a regulator of macroautophagy genes, Autophagy 12 (10) (2016) 1902–1916.
[39] M. Dodson, R. Castro-Portuguez, D.D. Zhang, NRF2 plays a critical role in mitigating lipid peroxidation and ferroptosis, Redox Biol. (2019), 101107.
[40] A. Anandhan, M. Dodson, C.J. Schmidlin, P. Liu, D.D. Zhang, Breakdown of an ironclad defense system: the critical role of NRF2 in mediating ferroptosis, Cell Chem Biol 27 (4) (2020) 436–447.
[41] G.A. Baselli, O. Jamialahmadi, S. Pelusi, E. Ciociola, F. Malvestiti, M. Saracino, L. Santoro, A. Cherubini, P. Dongiovanni, M. Maggioni, C. Bianco, F. Tavaglione, A. Cespiati, R.M. Mancina, R. D'Ambrosio, V. Vaira, S. Petta, L. Miele, U. Vespasiani-Gentilucci, A. Federico, J. Pihlajamaki, E. Bugianesi, A. L. Fracanzani, H.L. Reeves, G. Soardo, D. Prati, S. Romeo, L.V. Valenti, E. S. Investigators, Rare ATG7 genetic variants predispose patients to severe fatty liver disease, J. Hepatol. 77 (3) (2022) 596–606.
[42] D.D. Zhang, E. Chapman, The role of natural products in revealing NRF2 function, Nat. Prod. Rep. 37 (6) (2020) 797–826.
[43] L. Hu, S. Magesh, L. Chen, L. Wang, T.A. Lewis, Y. Chen, C. Khodier, D. Inoyama, L. J. Beamer, T.J. Emge, J. Shen, J.E. Kerrigan, A.N. Kong, S. Dandapani, M. Palmer, S.L. Schreiber, B. Munoz, Discovery of a small-molecule inhibitor and cellular probe of Keap1-Nrf2 protein-protein interaction, Bioorg. Med. Chem. Lett 23 (10) (2013) 3039–3043.
[44] T.G. Davies, W.E. Wixted, J.E. Coyle, C. Griffiths-Jones, K. Hearn, R. McMenamin, D. Norton, S.J. Rich, C. Richardson, G. Saxty, H.M. Willems, A.J. Woolford, J. E. Cottom, J.P. Kou, J.G. Yonchuk, H.G. Feldser, Y. Sanchez, J.P. Foley, B. J. Bolognese, G. Logan, P.L. Podolin, H. Yan, J.F. Callahan, T.D. Heightman, J. K. Kerns, Monoacidic inhibitors of the kelch-like ECH-associated protein 1: nuclear factor erythroid 2-related factor 2 (KEAP1:NRF2) protein-protein interaction with high cell potency identified by fragment-based discovery, J. Med. Chem. 59 (8) (2016) 3991–4006.
[45] D. Norton, W.G. Bonnette, J.F. Callahan, M.G. Carr, C.M. Griffiths-Jones, T. D. Heightman, J.K. Kerns, H. Nie, S.J. Rich, C. Richardson, W. Rumsey, Y. Sanchez, M.L. Verdonk, H.M.G. Willems, W.E. Wixted, L. Wolfe 3rd, A.J. Woolford, Z. Wu, T. G. Davies, Fragment-guided discovery of pyrazole carboxylic acid inhibitors of the kelch-like ECH-associated protein 1: nuclear factor erythroid 2 related factor 2 (KEAP1:NRF2) protein-protein interaction, J. Med. Chem. 64 (21) (2021) 15949–15972.